Cerebral Cortex November 2011;21:2565–2577
doi:10.1093/cercor/bhr039
Advance Access publication April 5, 2011

Diffusion Tensor Tractography Reveals Disrupted Topological Efficiency in White Matter Structural Networks in Multiple Sclerosis

Ni Shu[1], Yaou Liu[2], Kuncheng Li[2], Yunyun Duan[2], Jun Wang[1], Chunshui Yu[2], Huiqing Dong[3], Jing Ye[3] and Yong He[1]

[1]State Key Laboratory of Cognitive Neuroscience and Learning, Beijing Normal University, Beijing 100875, China, [2]Department of Radiology and [3]Department of Neurology, Xuanwu Hospital, Capital Medical University, Beijing 100053, China

Ni Shu and Yaou Liu have contributed equally to this work

Address correspondence to Dr Yong He, State Key Laboratory of Cognitive Neuroscience and Learning, Beijing Normal University, Beijing 100875, China. Email: yong.he@bnu.edu.cn.

Little is currently known about the alterations in the topological organization of the white matter (WM) structural networks in patients with multiple sclerosis (MS). In the present study, we used diffusion tensor imaging and deterministic tractography to map the WM structural networks in 39 MS patients and 39 age- and gender-matched healthy controls. Graph theoretical methods were applied to investigate alterations in the network efficiency in these patients. The MS patients and the controls exhibited efficient small-world properties in their WM structural networks. However, the global and local network efficiencies were significantly decreased in the MS patients compared with the controls, with the most pronounced changes observed in the sensorimotor, visual, default-mode, and language areas. Furthermore, the decreased network efficiencies were significantly correlated with the expanded disability status scale scores, the disease durations, and the total WM lesion loads. Together, the results suggest a disrupted integrity in the large-scale brain systems in MS, thus providing new insights into the understanding of MS connectome. Our data also suggest that a topology-based brain network analysis can provide potential biomarkers for disease diagnosis and for monitoring the progression and treatment effects for patients with MS.

Keywords: brain network, connectome, diffusion tensor imaging, multiple sclerosis

Introduction

Multiple sclerosis (MS) is an inflammatory, demyelinating disease of the central nervous system that is usually accompanied by impairments in motor, sensory, visual, and cognitive functions. These dysfunctions arise from disrupted neuronal conduction due to white matter (WM) lesions (Rovaris, Gass, et al. 2005; Filippi and Rocca 2008). In the past decade, modern brain imaging techniques, ranging from structural *magnetic resonance imaging (*MRI) to functional MRI, have been extensively used to assess the regional changes in brain structures and functions in patients with MS (Barkhof et al. 1998; Dalton et al. 2004; Rovaris et al. 2006; Charil et al. 2007; Ceccarelli et al. 2008; Dineen et al. 2009).

Diffusion tensor imaging (DTI) is a powerful noninvasive imaging technique that can be used to investigate WM microstructures. When applied to the brain, this technique has the potential to map the WM integrity and the structural connectivity in vivo (Basser et al. 2000). In recent years, DTI has been increasingly applied to the brain WM studies in MS. For example, researchers have shown that MS patients exhibited reduced WM integrity in the whole brain (Cercignani et al. 2001; Yu et al. 2008) and specific tracts such as the corticospinal tract, the optic radiation, and the corpus callosum (Lin et al. 2007; Ceccarelli et al. 2009; Dineen et al. 2009; Roosendaal et al. 2009). These studies provide a potential mechanism of the structural disconnections in the brain of MS patients.

Despite these advances, very little is known about the alterations in the topological organization of the WM networks in MS patients. Recent studies have suggested that the human WM networks can be mapped using diffusion MRI tractography methods and can be further described using graph theoretical analysis (for reviews, see Bullmore and Sporns 2009; He and Evans 2010). In healthy populations, the WM networks have been mapped using deterministic (Hagmann et al. 2008; Gong, He, et al. 2009; Shu et al. 2009) or probabilistic tractography methods (Iturria-Medina et al. 2008; Gong, Rosa-Neto, et al. 2009; Zalesky and Fornito 2009). The resultant networks exhibit important topological properties such as small-worldness and highly connected hubs regions in the posterior medial cortical regions. These studies have accelerated our understandings of human connectome in health and disease (Sporns et al. 2005). To our knowledge, only one study has examined the topological alterations in the brain networks in patients with MS, which were obtained by calculating cross-correlations in the gray-matter thickness derived from structural MRI (He et al. 2009). Yet, no studies reported MS-related changes in the WM structural networks.

Here, we used DTI tractography and graph theoretical approaches to investigate the topological organization of the WM networks in patients with MS and healthy comparisons. Given widespread disconnections previously reported in MS, we hypothesized that 1) patients with MS would show a decreased topological efficiency in the WM networks and that 2) these decreases would correlate with the clinical characteristics of the disease such as the expanded disability status scale (EDSS) scores, disease durations, and total WM lesion loads (TWMLLs).

Materials and Methods

Participants

This study included 39 MS patients (27 females; mean age 37.1 ± 10.7 years) and 39 age- and gender-matched healthy controls (HCs) (27 females; mean age 34.4 ± 9.9 years). All the patients were diagnosed as clinically definite relapsing-remitting multiple sclerosis (RRMS) (Lublin and Reingold 1996; Polman et al. 2005). The HCs had normal findings on the neurological examination and had no history of neurological dysfunction. All the participants were assessed clinically by experienced neurologists, who were unaware of the MRI results. None of the patients had been treated with related medications (e.g.,

corticosteroids or immunosuppressants) within the 3 months preceding the MRI scan. Table 1 shows the main demographics and the clinical characteristics of all the participants. Written informed consent was obtained from each participant, and this study was approved by the institutional review board of Xuanwu Hospital.

Image Acquisition

All participants were scanned with a 1.5T MRI scanner (Sonata, Siemens Medical Systems). T_2, T_1, and DTI images were acquired using with the following sequences: 1) T_2-weighted turbo spin echo imaging (repetition time [TR]/echo time [TE] = 5460/94 ms; number of excitation [NEX] = 3; echo train length = 11; matrix = 224 × 256; field of view [FOV] = 210 × 240 mm; slice = 30; slice thickness = 4 mm; orientation = axial), 2) T_1-weighted spin echo imaging (TR/TE = 1900/4 ms; NEX = 1; matrix = 224 × 256; FOV = 220 × 250 mm; slices = 96; slice thickness = 1.7 mm; orientation = sagittal), and 3) spin echo single-shot echo planar imaging (TR/TE = 5000/100 ms; NEX = 10; matrix = 128 × 128; FOV = 240 × 240 mm; slices = 30; slice thickness = 4 mm; orientation = axial; 6 nonlinear diffusion weighting gradient directions with b = 1000 s/mm^2 and 1 additional image without diffusion weighting [i.e., b = 0 s/mm^2]).

Measurement of Total WM Lesion Loads

The WM lesions of each patient were manually delineated on the T_2-weighted images by an experienced radiologist, who was blind to the clinical details (Y.L.). The lesions were redelineated on 2 separate occasions (at least 3-months apart) in 10 of the patients, and the intrarater reliability was 94.3%. We then obtained a binary lesion mask for each patient by setting the values within the WM lesions to 1 and 0 otherwise. To account for the effect of head size, we performed the following steps using the SPM8 package. First, the individual T_1-weighted images were coregistered to the T_2-weighted images using a linear transformation. Next, the transformed T_1 images were normalized to the ICBM152 T_1 template in the Montreal Neurological Institute (MNI) space using a nonlinear transformation. Last, the transformation information was applied to the lesion masks. This procedure yielded the relative TWMLL for each patient after the removal of the head size effect by the normalization process. To visualize the distribution of the WM lesions, we generated an average lesion map in which the value in a given voxel represented the proportion of the patients with a lesion (Fig. 1).

Table 1
Demographics and clinical characteristics of all participants

Characteristics	Patients (n = 39)	Controls (n = 39)	P values
Mean age (range) (years)	37.1 (18–58)	34.4 (18–58)	0.25
Gender (M/F)	12/27	12/27	>0.99
Median EDSS (range)	2.0 (1.0–6.0)	—	—
Median disease duration (range) (months)	36 (3–204)	—	—
Median TWMLL (range) (ml) (normalized)	4.6 (0.1–39.2)	—	—

Network Construction

Nodes and edges are the 2 basic elements of a network. In this study, we defined all the network nodes and edges using the following procedures.

Network Node Definition

The procedure of defining the nodes has been previously described (Gong, He, et al. 2009; Gong, Rosa-Neto, et al. 2009; Shu et al. 2009) and was performed in the present study using the SPM8. Briefly, individual T_1-weighted images were coregistered to the b0 images in the DTI space. The transformed T_1 images were then nonlinearly transformed to the ICBM152 T_1 template in the MNI space. The inverse transformations were used to warp the automated anatomical labeling atlas (Tzourio-Mazoyer et al. 2002) from the MNI space to the DTI native space. Of note, discrete labeling values were preserved by the use of a nearest-neighbor interpolation method. Using this procedure, we obtained 90 cortical and subcortical regions (45 for each hemisphere, see Table 2), each representing a node of the network (Fig. 2).

WM Tractography

To reconstruct the whole-brain WM tracts, we performed the following steps. First, the eddy current distortions and the motion artifacts in the DTI data set were corrected by applying an affine alignment of the diffusion-weighted images to the b0 images using FMRIB's Diffusion Toolbox (FSL, version 4.1; www.fmrib.ox.ac.uk/fsl). After this process, the diffusion tensors were estimated by solving the Stejskal and Tanner equation (Basser et al. 1994; Westin et al. 2002), and the reconstructed tensor matrix was diagonalized to obtain 3 eigen values (λ_1, λ_2, λ_3) and their corresponding eigenvectors. The fractional anisotropy (FA) of each voxel was also calculated. DTI tractography was carried out using DTIstudio (version 3.0) based on the "fiber assignment by continuous tracking" method (Mori et al. 1999). All the tracts in the data set were computed by seeding each voxel with an FA greater than 0.2. The tractography was terminated if it turned an angle greater than 45 degrees or reached a voxel with an FA less than 0.2 (Mori et al. 2002). As a result, all the fiber pathways in the brain were constructed using the deterministic tractography method.

Network Edge Definition

To define the network edges, we selected a threshold value for the fiber bundles. Two regions were considered structurally connected at least 3 fibers with 2 end points were located in these 2 regions (Shu et al. 2009). Such a threshold selection reduced the risk of false-positive connections due to noise or the limitations in the deterministic tractography and simultaneously ensured the size of the largest connected component (i.e., 90) in the networks was observed across all the controls (Shu et al. 2009). In the present study, we also evaluated the effects of different thresholds on the network analysis by setting threshold values of the number of fiber bundles that ranged from 1 to 5. We found that this thresholding procedure did not significantly influence our results (for details, see the Supplementary Materials). After defining the network edges, both the weighted and unweighted network analyses were performed. For the weighted networks, we defined the fiber number (FN) and the mean FA values of the connected fibers between 2 regions as the weights of the network

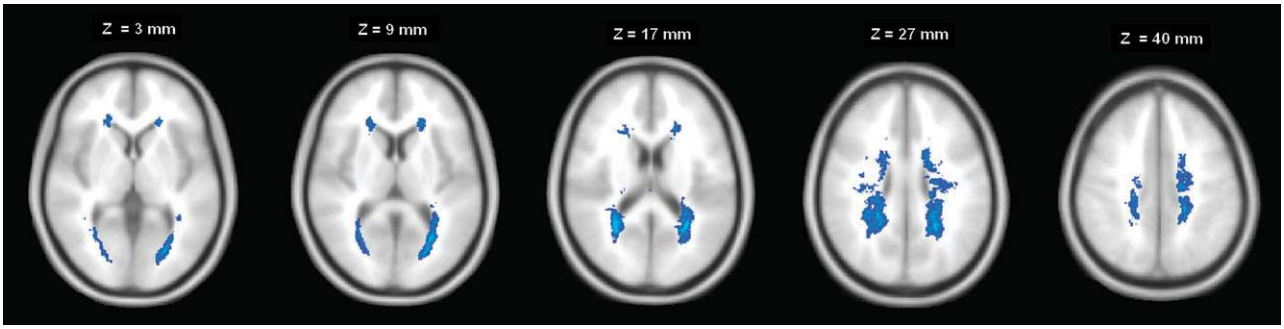

Figure 1. The mean WM lesion probability distribution that was thresholded at 10% is shown in blue and overlaid on the ICBM152 T_1 template in the MNI space.

Table 2
Cortical and subcortical regions of interest defined in the study

Index	Regions	Abbreviation	Index	Regions	Abbreviation
(1,2)	Precental gyrus	PreCG	(47,48)	Lingual gyrus	LING
(3,4)	Superior frontal gyrus, dorsolateral	SFGdor	(49,50)	Superior occipital gyrus	SOG
(5,6)	Superior frontal gyrus, orbital part	ORBsup	(51,52)	Middle occipital gyrus	MOG
(7,8)	Middle frontal gyrus	MFG	(53,54)	Inferior occipital gyrus	IOG
(9,10)	Middle frontal gyrus, orbital part	ORBmid	(55,56)	Fusiform gyrus	FFG
(11,12)	Inferior frontal gyrus, opercular part	IFGoperc	(57,58)	Postcentral gyrus	PoCG
(13,14)	Inferior frontal gyrus, triangular part	IFGtriang	(59,60)	Superior parietal gyrus	SPG
(15,16)	Inferior frontal gyrus, orbital part	ORBinf	(61,62)	Inferior parietal, but supramarginal and angular gyri	IPL
(17,18)	Rolandic operculum	ROL	(63,64)	Supramarginal gyrus	SMG
(19,20)	Supplementary motor area	SMA	(65,66)	Angular gyrus	ANG
(21,22)	Olfactory cortex	OLF	(67,68)	Precuneus	PCUN
(23,24)	Superior frontal gyrus, medial	SFGmed	(69,70)	Paracentral lobule	PCL
(25,26)	Superior frontal gyrus, medial orbital	ORBsupmed	(71,72)	Caudate nucleus	CAU
(27,28)	Gyrus rectus	REC	(73,74)	Lenticular nucleus, putamen	PUT
(29,30)	Insula	INS	(75,76)	Lenticular nucleus, pallidum	PAL
(31,32)	Anterior cingulate and paracingulate gyri	ACG	(77,78)	Thalamus	THA
(33,34)	Median cingulate and paracingulate gyri	DCG	(79,80)	Heschl gyrus	HES
(35,36)	Posterior cingulate gyrus	PCG	(81,82)	Superior temporal gyrus	STG
(37,38)	Hippocampus	HIP	(83,84)	Temporal pole: superior temporal gyrus	TPOsup
(39,40)	Parahippocampal gyrus	PHG	(85,86)	Middle temporal gyrus	MTG
(41,42)	Amygdala	AMYG	(87,88)	Temporal pole: middle temporal gyrus	TPOmid
(43,44)	Calcarine fissure and surrounding cortex	CAL	(89,90)	Inferior temporal gyrus	ITG
(45,46)	Cuneus	CUN			

Note: The regions are listed in terms of a prior template of an automated anatomical labeling-atlas (Tzourio-Mazoyer et al. 2002).

edges. For the unweighted networks, we considered the existence/absence of fiber bundles in which the network edges were defined as 1 if the FN between the 2 regions was larger than the threshold (3 in our case) and as 0 otherwise. As a result, for each participant, there were 3 different kinds of WM networks (FN-weighted, FA-weighted and binary), each of which was represented by a symmetric 90 × 90 matrix.

Network Analysis

Network Strength

For a network (graph) G with N nodes and K edges, we calculated the strength of G as:

$$S_p(G)=\frac{1}{N}\sum_{i\in G} S(i),$$

where $S(i)$ is the sum of the edge weights w_{ij} (w_{ij} are the FN or FA values for the weighted networks and 1 for the binary networks) linking to node i. The strength of a network is the average of the strengths across all the nodes in the network.

Small-World Efficiency

The small-world network parameters (the clustering coefficient and the shortest path length) were originally proposed by Watts and Strogatz (1998). In the present study, we employed a single network efficiency measure (Latora and Marchiori 2001) to quantify the small-world behavior of the WM structural networks. This efficiency metric deals with disconnected graphs and provides a clear physical meaning for the topological characterization of the networks. The global efficiency of G can be computed as (Latora and Marchiori 2001):

$$E_{glob}(G)=\frac{1}{N(N-1)}\sum_{i\neq j\in G}\frac{1}{L_{ij}},$$

where L_{ij} is the shortest path length between node i and j in G. The path length between node i and node j is defined as the sum of the edge lengths along this path, where each edge's length was obtained by computing the reciprocal of the edge weight, $1/w_{ij}$. The shortest path length L_{ij} between node i and j is the length of the path with the shortest length between the 2 nodes. The local efficiency of G is measured as (Latora and Marchiori 2001):

$$E_{\mathrm{loc}}(G)=\frac{1}{N}\sum_{i\in G} E_{\mathrm{glob}}(G_i),$$

where G_i denotes the subgraph composed of the nearest neighbors of node i. Practically, a network can be categorized as a small-world network if E_{glob} is slightly less than and E_{loc} is much greater than the matched random networks. Here, random networks were generated using the random rewiring procedure, described by Maslov and Sneppen (2002), that preserves the degree distribution as real networks. In particular, we retained the weight of each edge during the rewiring procedure such that the weight distribution of the network was preserved. For comparison purposes, we generated 500 random networks. Typically, a small-world network should meet the following criteria: $E_{\mathrm{loc}}(G)/E_{\mathrm{loc}}(G_{\mathrm{random}}) > 1$, $E_{\mathrm{glob}}(G)/E_{\mathrm{glob}}(G_{\mathrm{random}}) \approx 1$.

Regional Nodal Characteristics

To determine the nodal (regional) characteristics of the WM networks, we computed the regional efficiency, $E_{\mathrm{nodal}}(i)$ (Achard and Bullmore 2007):

$$E_{\mathrm{nodal}}(i)=\frac{1}{N-1}\sum_{i\neq j\in G}\frac{1}{L_{\mathrm{ij}}},$$

where L_{ij} is the shortest path length between node i and j in G. $E_{\mathrm{nodal}}(i)$ measures the average shortest path length between a given node i and all the other nodes in the network. The node i was considered a brain hub if $E_{\mathrm{nodal}}(i)$ was at least 1 standard deviation (SD) greater than the average nodal efficiency of the network (i.e., $E_{\mathrm{nodal}}(i)$ > mean + SD).

Statistical Analysis

To determine whether there were significant differences in the topological organization of the WM networks between the 2 groups, a multiple linear regression analysis was performed on each network metric (S_{p}, E_{glob}, E_{loc}, and E_{nodal}). Age and gender were entered as covariates of no interest in the models. To evaluate the clinical correlates of these network changes in the MS patients, we performed multiple linear regression analyses in which the network parameters (S_{p}, E_{glob}, E_{loc}, and E_{nodal}) were considered to be dependent variables, and the clinical variables (the EDSS scores, disease durations, and TWMLL) were considered to be independent variables. Age and gender were regressed out as covariates. For the clinical relevance analysis of the nodal properties, we only included the regions with significant between-group differences in their nodal efficiencies.

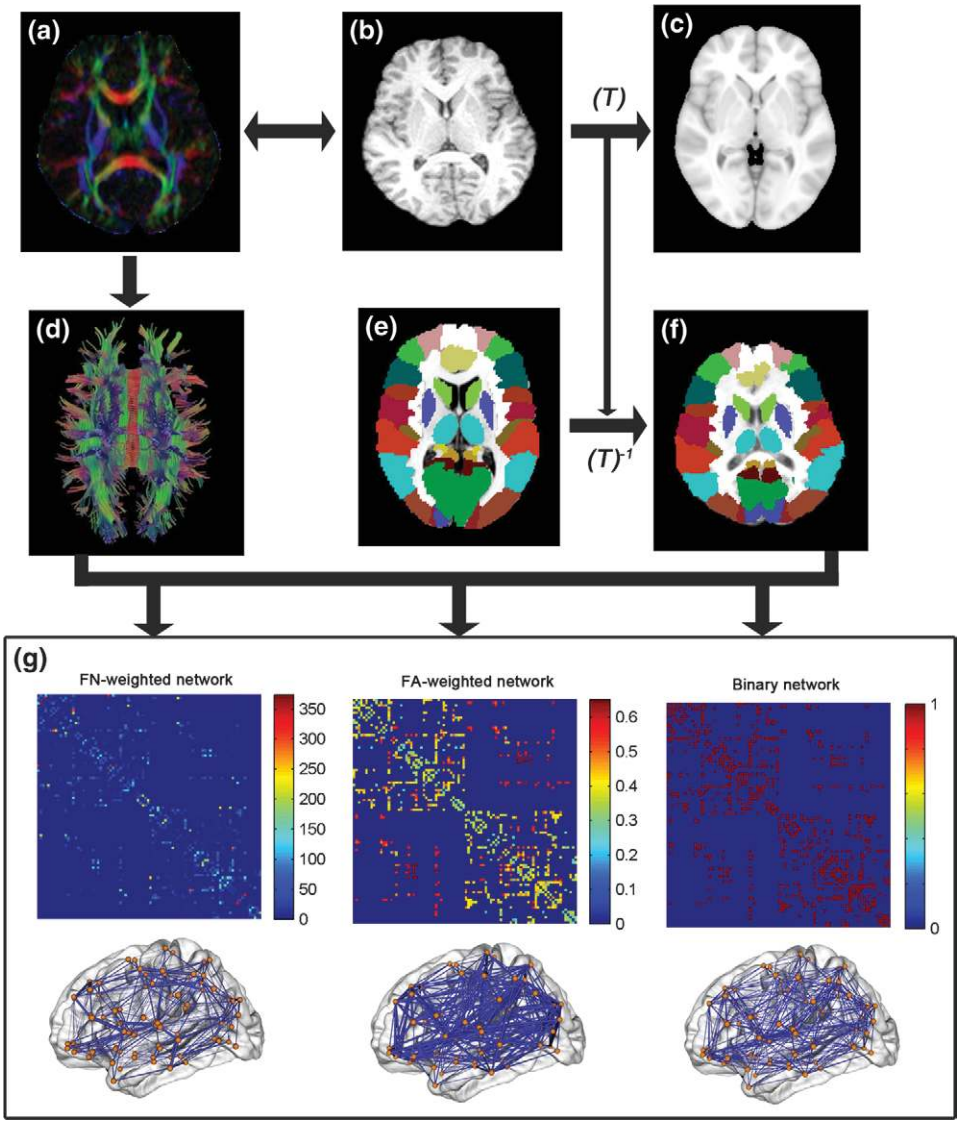

Figure 2. A flowchart for the construction of WM structural network by DTI. 1) The rigid coregistration from the T_1-weighted structural MRI (*b*) to DTI native space (*a*) (DTI color-coded map; red, left to right; green, anterior to posterior; blue, inferior to superior) for each subject. 2) The nonlinear registration from the resultant structural MRI to the ICBM152 T_1 template in the MNI space (*c*), resulting in a nonlinear transformation (T). 3) The application of the inverse transformation (T^{-1}) to the automated anatomical labeling template in the MNI space (*e*), resulting in the subject-specific automated anatomical labeling mask in the DTI native space (*f*). All registrations were implemented in the SPM8 package. 4) The reconstruction of all the WM fibers (*d*) in the whole brain using DTI deterministic tractography in DTIstudio. 5) The weighted networks of each subject (*g*) were created by computing the FN-weighted and the mean FA values (FA-weighted) of the fiber bundles that connected each pair of brain regions. The binary network was created by considering the existence/absence of fiber bundles between 2 regions. The matrices and 3D representations (lateral view) of the 3 kinds of WM structural networks of a representative healthy subject were shown in the bottom panel. The nodes are located according to their centroid stereotaxic coordinates, and the edges are coded according to their connection weights. For details, see the Materials and Methods section.

To further explore whether there were specific correlations between topological changes of WM networks and behavior deficits, we selected a subset of patients (11/39 patients) mainly with visual dysfunction symptom. A multiple linear regression analysis was performed on each network metric (S_p, E_{glob}, E_{loc}, and E_{nodal}) to reveal how topological efficiencies of WM networks in this subset of patients differed from those of the controls. Age and gender were entered as covariates of no interest in the models.

Reproducibility

To test the reproducibility of our findings, we used a split-half method. Briefly, we divided the HC group into 2 subgroups according to the distributions of age and gender: HC1: 19 participants, 13 females, age (mean ± SD) 34.1 ± 9.6 years; HC2: 20 participants, 14 females, age (mean ± SD) 34.8 ± 10.5 years. As such, we divided the MS group into 2 subgroups (MS1: 19 participants, 13 females, age [mean ± SD] 37 ± 10.4 years; MS2: 20 participants, 14 females, age [mean ± SD] 37.3 ± 11.3 years). There were no significant differences (all $P > 0.1$) in the age and the sex between any 2 groups. To determine whether there was a consistent topological organization in the population, we computed Pearson's correlation coefficients for the nodal efficiency of the WM networks between HC1 and HC2 subgroups and between MS1 and MS2 subgroups. We also compared the topological parameters (S_p, E_{glob}, and E_{loc}) between each pair of subgroups using linear regression analyses. The age and gender effects were removed in these analyses.

Results

In the present study, we constructed 3 different kinds of networks for each participant, including FN-weighted, FA-

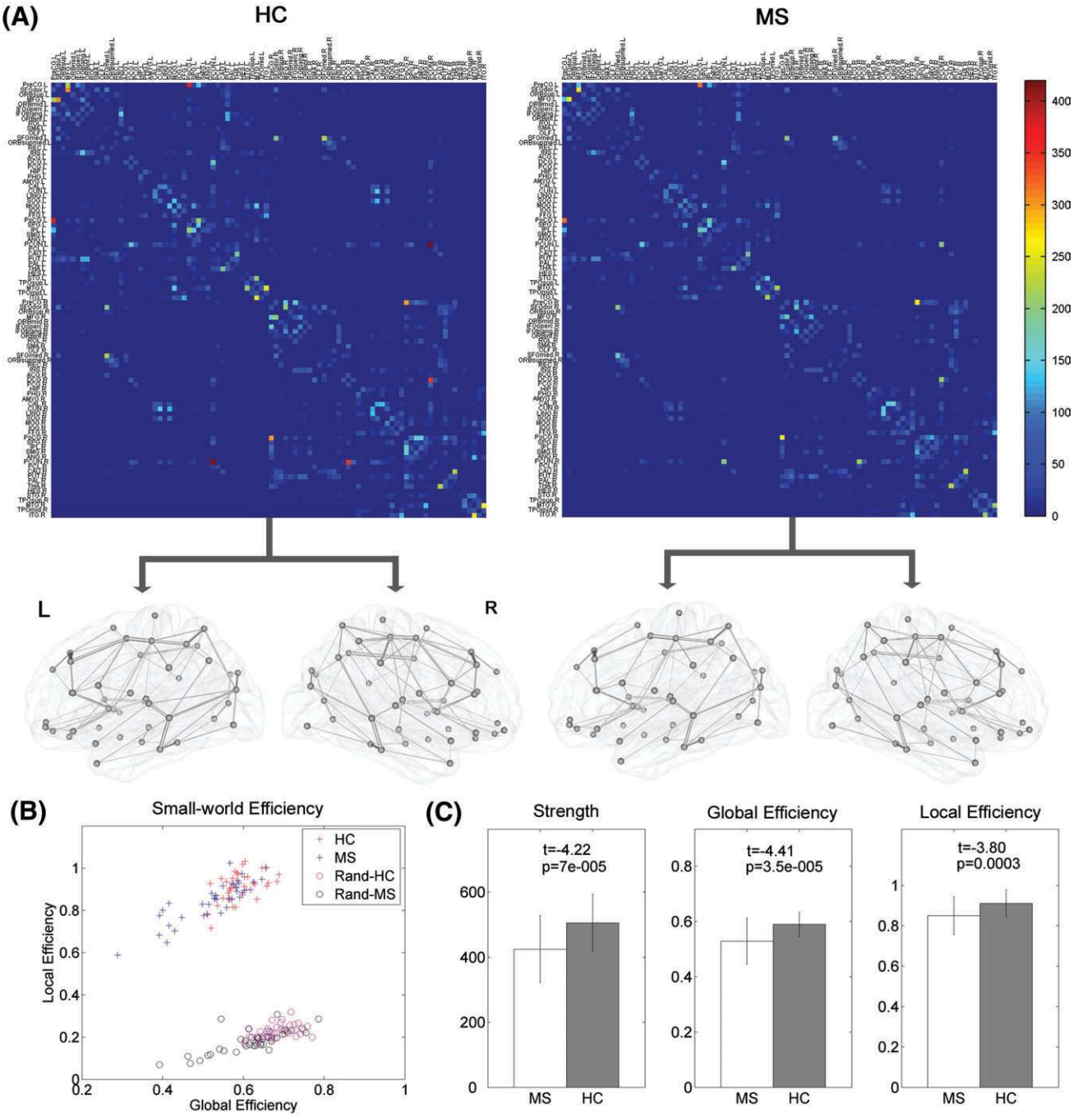

Figure 3. Small-world efficiency of WM networks and between-group differences. (*A*) The mean matrices and the 3D representations of the WM structural networks of the HC and MS groups. Notably, the networks shown here were constructed by averaging the anatomical connection matrices of all subjects in each group. The nodal regions are located according to their centroid stereotaxic coordinates. The edge widths represent the connection weights between nodes. (*B*) The small-world characteristics of the WM structural networks in the HC and MS groups, which have a much higher local efficiency and a similar global efficiency compared with the matched random networks (Rand-HC and Rand-MS). (*C*) Between-group differences in the strength, global efficiency, and local efficiency of the WM structural networks. The bars represent the mean values and error bars represent the SDs of the network parameters in each group. Note that the MS patients showed reduced strength, global efficiency, and local efficiency in the brain networks compared with the controls ($P = 0.05$).

weighted, and binary networks (Fig. 2). Despite the different connectivity metrics of the networks, we observed compatible results for the group differences and the clinical correlations. In the present study, we focused mainly on the results that were obtained from the analyses of the FN-weighted networks (for the other results of the FA-weighted and binary networks, see the Supplementary Materials).

Small-World Efficiency of the WM Networks

Small-World Efficiency

Using graph theoretical analyses, we showed that the WM structural networks of both the HC and MS groups exhibited a much higher local efficiency and a similar global efficiency compared with the matched random networks [HC group:

$E_{loc}(G)/E_{loc}(G_{random})$ = 4.14, $E_{glob}(G)/E_{glob}(G_{random})$ = 0.87; MS group: $E_{loc}(G)/E_{loc}(G_{random})$ = 5.05, $E_{glob}(G)/E_{glob}(G_{random})$ = 0.85] (Fig. 3). The results suggest that there are small-world characteristics of the WM structural networks in the HC and MS groups.

Group Differences in Network Efficiency

For each participant, we calculated the strength, global, and local efficiency of the WM networks. Compared with HCs, the MS patients exhibited significant decreases in the strength (t_{74} = −4.22, $P = 7 \times 10^{-5}$), global efficiency (t_{74} = −4.41, $P = 3.5 \times 10^{-5}$), and local efficiency (t_{74} = −3.80, P = 0.0003) of their WM structural networks (Fig. 3).

Regional Efficiency of the WM Networks

Hub Regions

In the HC group, we identified 14 hub nodes in the WM structural networks, including 8 association cortex regions, 4 primary cortex regions, 1 paralimbic cortex region, and 1 subcortical region (Fig. 4 and Supplementary Table S5). In the MS group, we identified 15 hub regions, including 8 association cortex regions, 4 primary cortex regions, and 3 subcortical regions (Fig. 4 and Supplementary Table S5). Of note, 13 of the hub regions were the same for both groups, including the bilateral precuneus (PCUN), bilateral precentral gyrus (PreCG), bilateral postcentral gyrus (PoCG), bilateral dorsolateral superior frontal gyrus (SFGdor), bilateral middle frontal gyrus (MFG), left medial superior frontal gyrus (SFGmed), left putamen (PUT), and left inferior parietal gyrus (IPL). One brain region, the right median cingulate and paracingulate gyrus (DCG), was identified as a hub in the HC group but not in the MS group. Two brain regions, the right PUT and the right thalamus (THA), were identified as hubs in the MS group but not in the HC group. The results suggest that the hubs that we identified for both groups were predominantly in the regions of the association cortices that receive convergent inputs from multiple cortical regions (Mesulam 1998). These results are consistent with those from previous studies (He et al. 2007; Hagmann et al. 2008; Iturria-Medina et al. 2008; Gong, He, et al. 2009).

Group Differences in Regional Efficiency

Compared with the controls, the MS patients exhibited a widespread reduction in the nodal efficiency in many brain regions [$P < 0.05$, false discovery rate (FDR)-corrected]. These regions can be categorized into 4 different functional systems: 1) the sensorimotor system, including the bilateral PreCG, the right PoCG, and the left paracentral lobule (PCL); 2) the visual system, including the bilateral superior occipital gyri (SOG), the right cuneus (CUN), and the left middle occipital gyrus (MOG); 3) the default-mode system, including the left posterior cingulate gyrus (PCG), the bilateral PCUN, the right anterior cingulate gyrus (ACG), the right DCG, and the right IPL; and

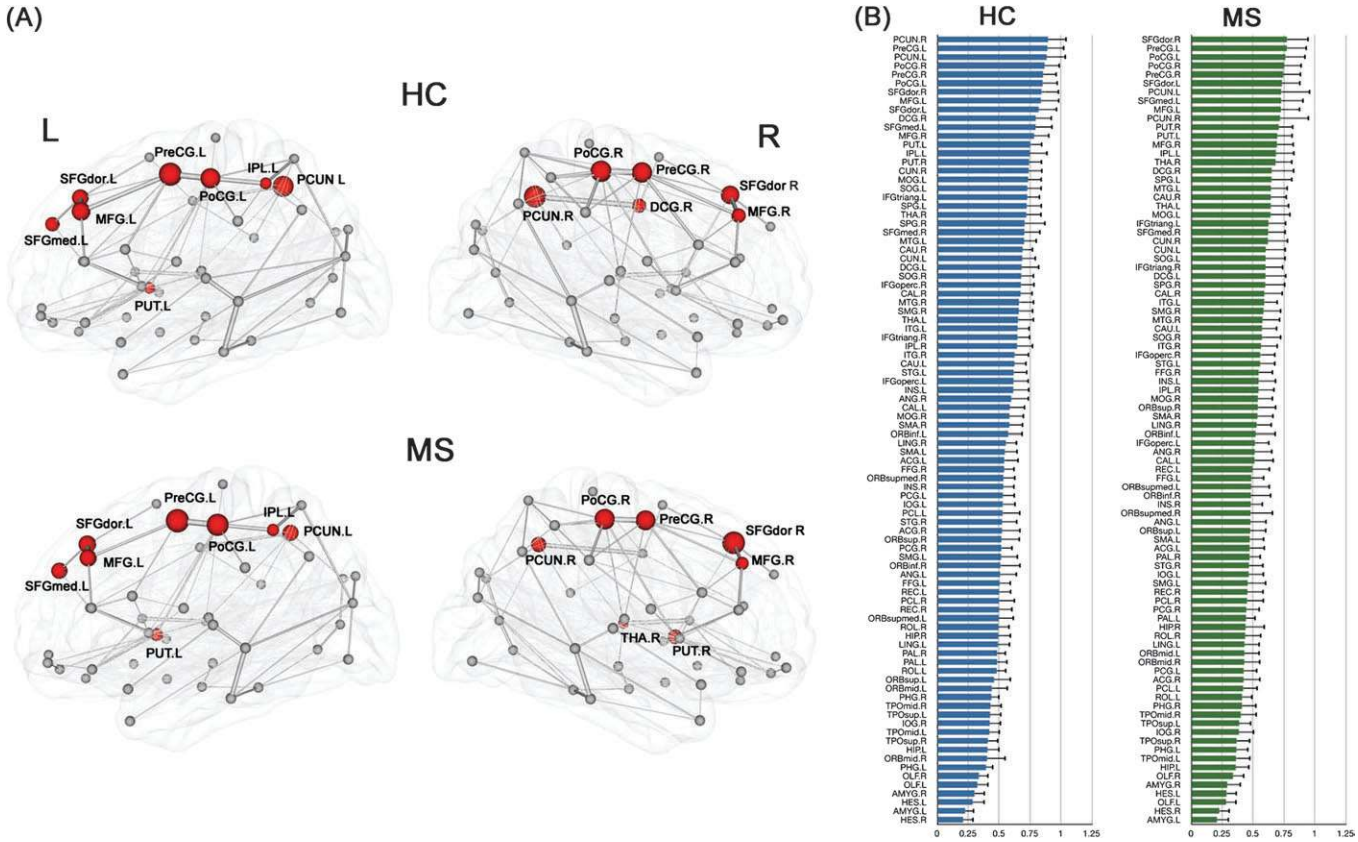

Figure 4. The hub region distributions in the WM structural networks of the HC and MS groups. (*A*) 3D representations of the hub distributions in the HC and MS groups. The hub nodes are shown in red with node sizes indicating their nodal efficiency values. The regions were mapped onto the cortical surface at the lateral view. Notably, the networks shown here were constructed by averaging the anatomical connection matrices of all subjects in each group. The nodal regions are located according to their centroid stereotaxic coordinates. The edge widths represent the connection weights between nodes. (*B*) The 90 brain regions are sorted by using mean nodal efficiencies in descending order for each group (left, HC group; right, MS group). For the abbreviations of nodes, see Table 2.

4) the language system, including the bilateral opercular parts of the inferior frontal gyrus (IFGoperc), the left rolandic operculum (ROL), the left triangular part of the inferior frontal gyrus (IFGtriang), and the bilateral MFG (Table 3 and Fig. 5).

For the subset of MS patients with visual deficits, we found that the patients showed reduced small-world network efficiency as compared with the controls (E_{glob}: $t_{46} = -3.73$, $P = 5.3 \times 10^{-4}$; E_{loc}: $t_{46} = -2.36$, $P = 0.023$). Moreover, the distribution of regions with reduced efficiency ($P < 0.05$, FDR-corrected) was similar with the results derived from the analysis in all patients. Notably, the region with most significantly reduced efficiency was located in the left SOG in the subset of patients (with visual dysfunction) (Supplementary Table S7).

The Correlation between the Network Efficiency and Clinical Variables

Using multiple linear regression analyses, we found that in MS patients, the global and local efficiencies of the WM structural networks were significantly correlated with their EDSS scores (E_{glob}: $t_{35} = -2.37$, $P = 0.023$; E_{loc}: $t_{35} = -2.33$, $P = 0.026$), disease durations (E_{glob}: $t_{35} = -2.76$, $P = 0.0091$; E_{loc}: $t_{35} = -2.42$, $P = 0.021$), and TWMLL (E_{glob}: $t_{35} = -3.90$, $P = 0.00041$; E_{loc}: $t_{35} = -2.71$, $P = 0.010$) (Fig. 6).

Furthermore, we found that the nodal efficiencies of several brain regions had significant correlations with the EDSS scores (right CUN, bilateral PCUN, left PCL, left PCG, left ROL, left PreCG, right DCG, right MFG, and right SOG), disease durations (bilateral PCUN, left PCG, left ROL, right DCG, left IFGoperc,

Table 3
Brain regions with decreased nodal efficiency in patients with MS

Systems	Regions	*T* values of group differences (uncorrected *P* values)	*T* values of clinical correlations (*P* values)		
			EDSS	Disease duration	TWMLL
Sensorimotor	PCL.L	−3.77 (0.0003)	−2.56 (0.015)	—	−4.01 (0.0003)
	PreCG.R	−3.74 (0.0004)	—	—	−2.68 (0.011)
	PoCG.R	−3.70 (0.0004)	—	—	−2.61 (0.013)
	PreCG.L	−3.62 (0.0005)	−2.34 (0.025)	−2.18 (0.036)	−3.43 (0.002)
Visual	SOG.L	−4.11 (0.0001)	—	—	−2.78 (0.009)
	CUN.R	−3.85 (0.0003)	−3.19 (0.003)	—	−2.27 (0.030)
	SOG.R	−3.46 (0.0009)	−2.05 (0.048)	—	−2.61 (0.013)
	MOG.L	−3.23 (0.0019)	—	—	−3.39 (0.002)
Default-mode	PCG.L	−4.45 (0.00003)	−2.54 (0.016)	−2.71 (0.010)	−3.30 (0.002)
	DCG.R	−4.21 (0.0001)	−2.19 (0.036)	−2.47 (0.019)	—
	PCUN.R	−4.13 (0.0001)	−2.68 (0.011)	−2.84 (0.008)	−2.26 (0.030)
	ACG.R	−3.64 (0.0005)	—	—	—
	PCUN.L	−3.57 (0.0006)	−2.58 (0.014)	−3.12 (0.004)	−2.93 (0.006)
	IPL.R	−3.27 (0.0016)	—	—	−2.58 (0.014)
Language	IFGoperc.R	−4.54 (0.00002)	—	—	—
	ROL.L	−3.98 (0.0002)	−2.52 (0.017)	−2.60 (0.013)	−3.11 (0.004)
	IFGoperc.L	−3.77 (0.0003)	—	−2.46 (0.019)	−2.28 (0.029)
	IFGtriang.L	−3.55 (0.0007)	—	—	−2.10 (0.043)
	MFG.L	−3.48 (0.0008)	—	—	—
	MFG.R	−3.27 (0.0017)	−2.13 (0.040)	—	—

Note: The regions with significant group differences in the nodal efficiency at $P < 0.05$ (FDR-corrected) can be categorized into 4 functional systems, and they were listed in an ascending order by the *T* values in each system. For these regions, the nodal efficiencies of several of the regions have significant correlations with the EDSS scores, disease durations, and TWMLL at $P < 0.05$ (uncorrected). —, nonsignificant at $P < 0.05$.

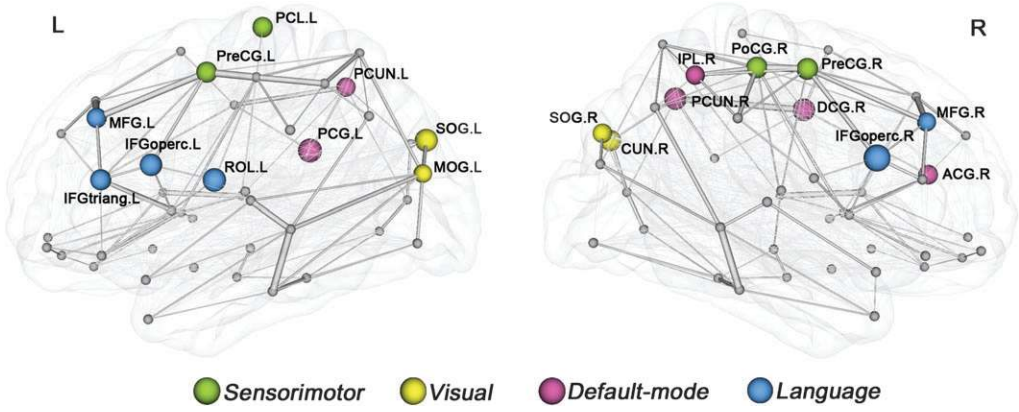

Figure 5. The brain regions with a significantly reduced efficiency in patients with MS. These regions can be categorized into 4 functional systems: 1) the nodes in green are within the sensorimotor system, including the bilateral PreCG, right PoCG, and left PCL; 2) the nodes in yellow are within the visual system, including the bilateral SOG, right CUN, and left MOG; 3) the nodes in red are within the default-mode system, including the left PCG, bilateral PCUN, right ACG, right DCG, and right IPL; and 4) the nodes in blue are within the language system, including the bilateral IFGoperc, left ROL, left IFGtriang, and bilateral MFG. All brain regions showed reduced regional efficiency at $P < 0.05$ (FDR-corrected). The node sizes indicate the significance of between-group differences in the regional efficiency. The network shown here was constructed by averaging the anatomical connection matrices of all HCs. The nodal regions are located according to their centroid stereotaxic coordinates. The edge widths represent the connection weights between nodes. For the abbreviations of nodes, see Table 2.

and left PreCG), and TWMLL (left PCL, bilateral PreCG, left MOG, left PCG, left ROL, bilateral PCUN, bilateral SOG, right PoCG, right IPL, left IFGoperc, right CUN, and left IFGtriang) (Table 3 and Fig. 7).

Reproducibility of Our Findings

As described above, we classified all the participants into 4 subgroups: 2 HC subgroups (HC1 and HC2) and 2 MS subgroups (MS1 and MS2). We then constructed the WM structural networks for each subgroup (Fig. 8). There were significant differences (all $P < 0.05$) in the global and local efficiencies when the HC and MS subgroups were compared (HC1 vs. MS1; HC1 vs. MS2; HC2 vs. MS1; HC2 vs. MS2) (Fig. 8 and Supplementary Table S6). However, we did not observe any significant differences in the global or local efficiencies between the 2 HC subgroups (HC1 vs. HC2, all $P > 0.1$) or between the 2 MS subgroups (MS1 vs. MS2, all $P > 0.1$) (Fig. 8 and Supplementary Table S6). A significant correlation was

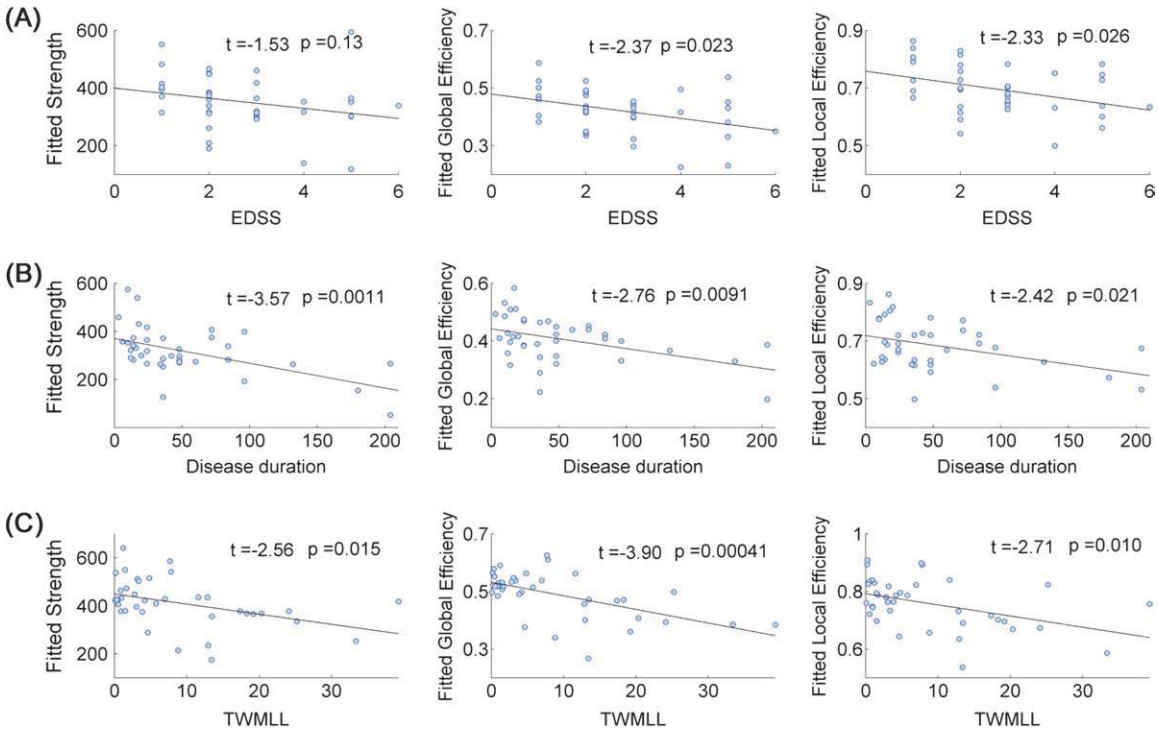

Figure 6. The correlations between the global network parameters and clinical variables in MS patients. (*A*) Plots showing the significant decreases of the global and local efficiencies of the network with EDSS scores. (*B*) Plots showing the significant decreases of the strength, global, and local efficiencies of the network with disease durations. (*C*) Plots showing the significant decreases of the strength, global, and local efficiencies of the network with TWMLL.

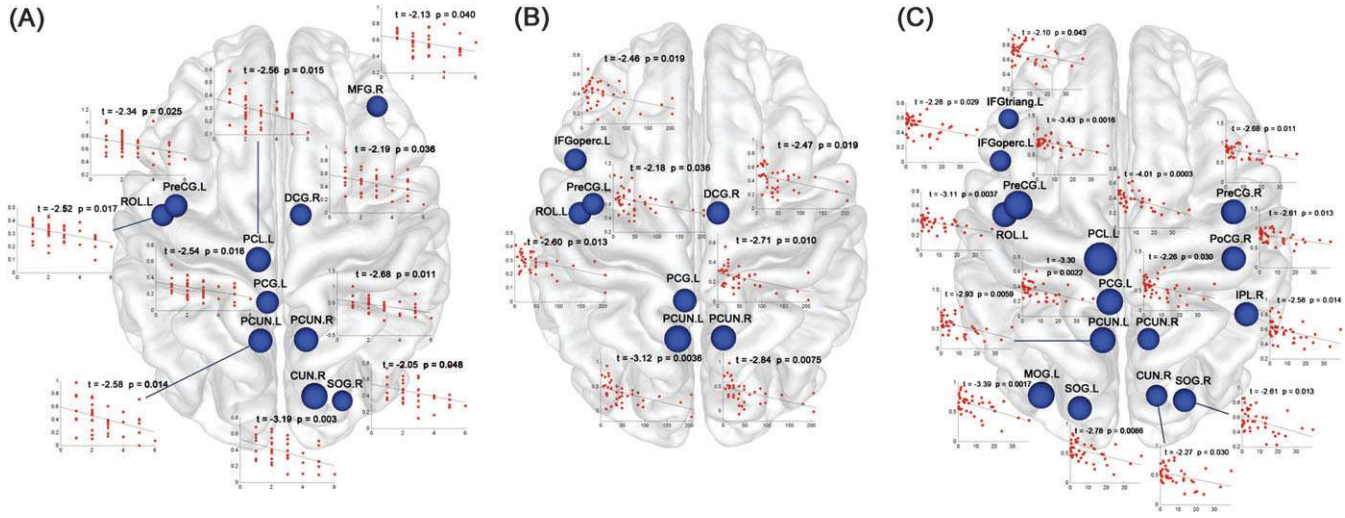

Figure 7. The regions with significant correlations between the nodal efficiencies and clinical variables in MS patients. The regions were overlaid on the brain surface at the axial view. The node sizes indicate the significance of the correlations between the nodal efficiencies and clinical variables. (*A*) Nodes and their plots showing the decreases of the nodal efficiencies with EDSS scores. (*B*) Nodes and their plots showing the decreases of the nodal efficiencies with disease durations. (*C*) Nodes and their plots showing the decreases of the nodal efficiencies with TWMLL. For the abbreviations of nodes, see Table 2.

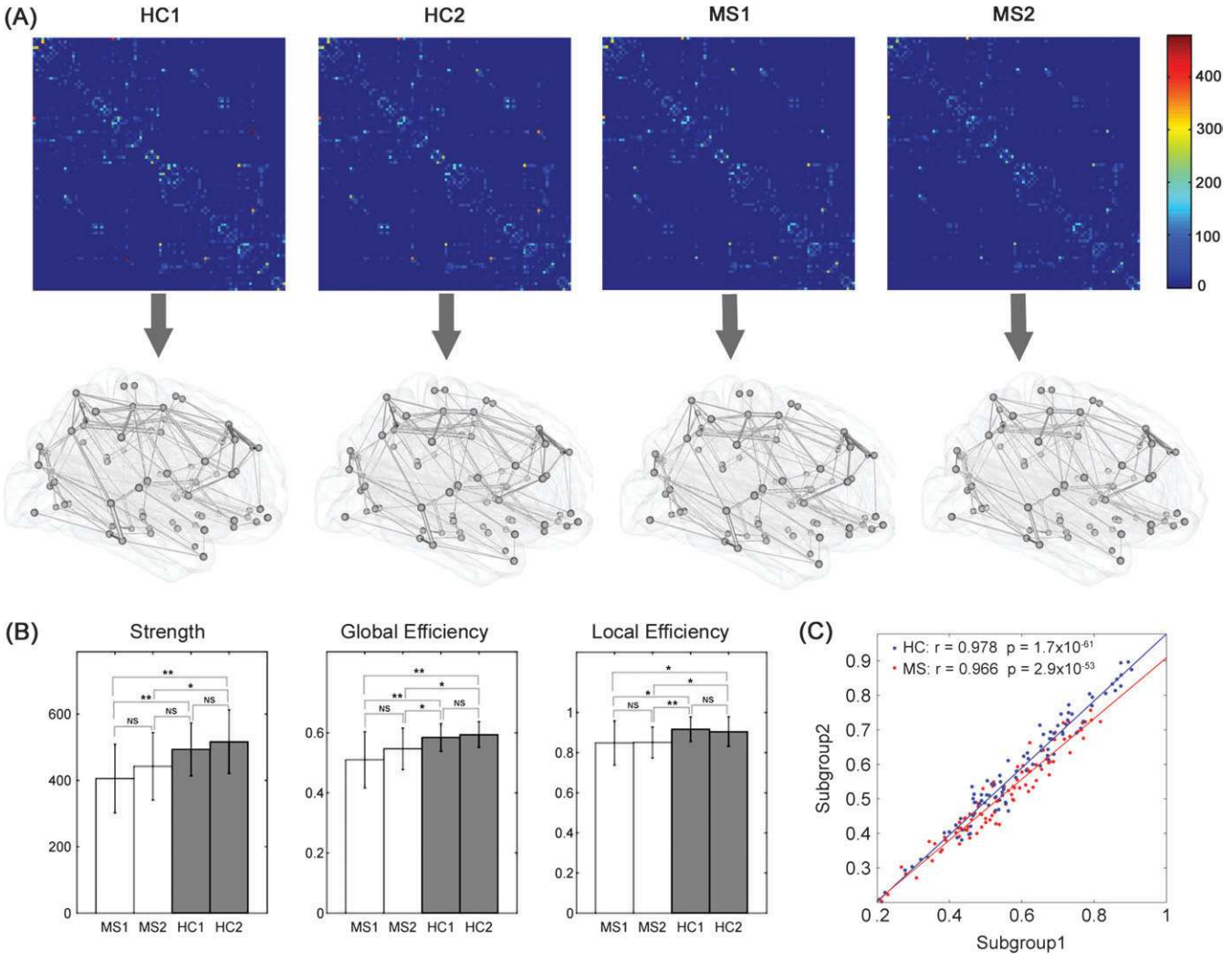

Figure 8. The evaluation of the reproducibility of the results. (*A*) The mean matrices and the 3D representations of the WM structural networks of each subgroup (HC1, HC2, MS1, and MS2). Notably, the networks shown here were constructed by averaging the anatomical connection matrices of all subjects in each subgroup. The nodal regions are located according to their centroid stereotaxic coordinates. The edge widths represent the connection weights between nodes. (*B*) Between-group differences in the global network parameters (strength, global efficiency, and local efficiency). The bars represent the mean values, and error bars represent the SDs of the network parameters in each subgroup. Note that there were significant differences in the global and local efficiencies when the HC and MS subgroups were compared (HC1 vs. MS1; HC1 vs. MS2; HC2 vs. MS1; HC2 vs. MS2). There were not any differences in the global or local efficiencies between the 2 HC subgroups (HC1 vs. HC2) or between the 2 MS subgroups (MS1 vs. MS2). $*P < 0.05$; $**P < 0.005$; NS, nonsignificant ($P > 0.05$). (*C*) Significant correlations in the nodal efficiencies between the 2 HC subgroups and between the 2 MS subgroups.

observed in the nodal efficiencies when the 2 HC subgroups were compared ($r = 0.978$; $P = 1.7 \times 10^{-61}$) and when the 2 MS subgroups were compared ($r = 0.966$; $P = 2.9 \times 10^{-53}$) (Fig. 8). These results suggest a high reproducibility of our findings.

Discussion

We investigated the WM networks of MS patients and HCs using DTI tractography and graph theoretical approaches. Both of groups exhibited efficient small-world properties in their WM networks. However, the topological efficiencies were significantly decreased in the patients compared with controls, with the most pronounced changes in the sensorimotor, visual, default-mode, and language areas. The decreases in the efficiency were significantly correlated with the EDSS scores, disease durations, and TWMLL. Together, our data show disrupted topological organizations of WM networks in patients with MS, which could be responsible for the functional disabilities in patients.

Disrupted Small-World Efficiencies in the WM Networks in MS

The human brain is a complex system with an optimal balance between local specialization and global integration. In this study, we identified the small-world properties of the WM networks in MS patients and controls, which were characterized by high global and local efficiencies. This finding is consistent with previous network studies based on different imaging techniques (for reviews, see Bullmore and Sporns 2009; He and Evans 2010).

Although there are small-world properties in the MS networks, the global and local efficiencies were significantly decreased compared with controls. The global efficiency reflects the information transfer between the remote cortical

regions, and it is mainly associated with long-range connections. The local efficiency is predominantly related to the short-range connections between neighboring regions. Decreases in both global and local efficiencies reflect disrupted topological organizations of the WM networks in patients with MS, which could be due to impaired structural connections. Our results can be supported by many previous studies. Evidence from a quantitative postmortem study showed a significant reduction in axonal density and the total number of axons in MS patients (Evangelou et al. 2000). Many DTI studies provided direct evidence for disrupted structural integrity in various WM tracts in MS patients, such as the corticospinal tract, the optic radiation, and the corpus callosum (Lin et al. 2007; Bodini et al. 2009; Ceccarelli et al. 2009; Reich et al. 2009). Moreover, functional MRI studies have showed abnormal functional integrity in MS (Rocca et al. 2007, 2010; Passamonti et al. 2009). These studies provide rich evidence for the structural and functional disconnectivity in patients with MS. Here, our data further supports the notion of MS as a disconnection syndrome from a network perspective.

Disrupted Nodal Efficiency in the WM Networks in MS

We observed reduced nodal efficiency in the MS networks. The involved regions were categorized into 4 distinct systems: sensorimotor, visual, default-mode, and language systems.

Sensorimotor System

We observed reduced nodal efficiencies in several regions related to sensorimotor functions (PreCG, PoCG, and PCL). Functional imaging studies observed abnormal neuronal activity in these sensorimotor regions in MS patients (Lowe et al. 2002, 2008; Rocca et al. 2010). Morphological studies also reported decreases of gray-matter volumes in these regions (Sailer et al. 2003; Charil et al. 2007; Ceccarelli et al. 2008). Using DTI analysis, abnormal diffusivity was observed in the sensorimotor pathways (e.g., the corticospinal tracts) (Lin et al. 2007; Reich et al. 2008; Rocca et al. 2010). These findings suggest that structural and functional changes exist in the sensorimotor system in patients with MS, which provides support for our findings.

Visual System

Reduced nodal efficiencies were also found in several occipital regions (SOG, MOG, and CUN) that are important for visual processing. The results are supported by the fact that the WM lesions identified in the patients are mainly located in the visual pathways (Fig. 1). In fact, previous DTI studies have revealed abnormal diffusion changes in the optic radiation in MS patients (Kolappan et al. 2009; Roosendaal et al. 2009; Dasenbrock et al. 2010). Additionally, Reich et al. (2009) found that the diffusion measures of the optic radiation were correlated with retinal injury and visual disability in MS patients. Moreover, gray matter atrophy of the optic pathways (Sepulcre et al. 2009), magnetic transfer ratio changes in the optic nerve (Kolappan et al. 2009), and decreased functional activation in the primary visual cortex (Faro et al. 2002) have also been reported in MS. Thus, our results provide further evidence for the disruption of the visual system in patients with MS.

Default-Mode System

We observed a decreased nodal efficiency in the MS networks in several default-mode regions (ACG, DCG, PCG, PCUN, and IPL). These regions are core components of the default-mode (DMN) and have been implicated in the processing of episodic memory (Raichle et al. 2001; Greicius et al. 2003). Relating to MS, functional MRI studies revealed that a dysfunction of the DMN was associated with a reduced cognitive performance (Roosendaal et al. 2010; Schoonheim et al. 2010). Using a combined DTI and functional MRI technique, Rocca et al. (2010) showed that the functional changes in the DMN were correlated with structural changes in the cingulum (a major WM structure that links cingulate regions). Thus, our results are in agreement with these previous findings.

Language System

Reduced nodal efficiencies were observed in several frontal regions (IFGoperc, IFGtriang, MFG, and ROL) that are key components for language processing. The IFGoperc and IFGtriang, comprising Broca's area, especially in the left hemisphere, are known to be important for language production. The MFG is responsible for writing (Lubrano et al. 2004; Roux et al. 2009), and the ROL is involved in speech (Indefrey et al. 2001). Structural and functional changes in the prefrontal regions in MS patients have been reported in previous neuroimaging studies (Au Duong, Audoin, et al. 2005; Au Duong, Boulanouar, et al. 2005; Dineen et al. 2009; He et al. 2009; Rocca et al. 2010), but the exploration of language-specific regions has not received much attention. In this study, 8/39 MS patients exhibited language deficits (including verbal influency and naming difficulty), which supports for our findings of the abnormalities in the language areas.

Interestingly, we found in the subset of patients mainly with visual dysfunction, the left SOG, one of regions for visual processing, showed most significantly reduced efficiency in the WM networks. However, when analyzing all the patients, the SOG was not the most affected region (Table 3). This additional analysis suggests that the topological changes of the WM networks could be associated with specific behavior deficits in the MS patients.

Clinical Relevance of Network Alterations in MS

We found that the global and local efficiencies of the WM networks were significantly correlated with the EDSS scores in MS patients. Using an region of interest-based analysis, Ciccarelli et al. (2001) reported a significant correlation between the EDSS scores and the FA values throughout the WM in MS patients. Here, we are the first to show the association between the motor disability and the structural organization in MS patients from a network perspective. Moreover, the disease durations were also correlated with the network efficiency, suggesting a longer duration of disease induced a more severe disruption in network topology. This finding is also supported by findings from previous DTI studies, which have shown a correlation between WM integrity and the disease duration in MS patients (Rovaris, Ballo, et al. 2005; Fink et al. 2010). We also observed that the network efficiencies were significantly correlated with the TWMLL in MS patients, suggesting that a disruption in network organization occurred as the lesion volume increased. The periventricular WM lesions cause damages to the myelin and axons connecting multiple cortical regions and further have an impact on the information transfer efficiency between distributed brain regions. This finding is consistent with our recent study using gray-matter

thickness network analyses (He et al. 2009). Moreover, this result is also compatible with the findings from DTI studies in which lesion volumes are significantly correlated with the FA values in the WM in patients with MS (Ciccarelli et al. 2003; Giorgio et al. 2010; Vishwas et al. 2010). Importantly, the efficiencies of several brain regions, such as the PCUN, PCG, PreCG, and ROL, are significantly correlated with all the clinical variables (the EDSS scores, disease durations, and TWMLL), implying that these regions play a key role in the clinical symptoms in MS patients. Together, our data suggests that the network efficiency metrics provide potential biomarkers for disease diagnosis for monitoring the progression and treatment effects for patients with MS.

Methodological Issues

Several issues need to be addressed. First, the present study used a suboptimal DTI sequence with 6 diffusion-encoding gradient directions and nonisotropic voxel size. Using a split-half analysis, we found that the results showed a high reproducibility across subjects. It suggests that our findings are reliable, although some suboptimal scanning parameters were used here. Using similar scanning sequences, a recent study also reported a high reproducibility of the WM network properties (Gong, He, et al. 2009). Nonetheless, the analysis should be performed on the new data sets derived from optimal scanning parameters to further evaluate the reproducibility of our results. Second, we employed deterministic tractography to define the edges of the WM networks. This method has been used in previous DTI studies (Gong, He, et al. 2009; Shu et al. 2009). However, the tracking procedure always stops when it reaches regions with fiber crossings and low FA values because of the "fiber crossing" problem (Mori and van Zijl 2002), which might result in a loss of existing fibers. Other studies have proposed the use of probabilistic tractography to define the network edges (Iturria-Medina et al. 2008; Gong, Rosa-Neto, et al. 2009), which could be helpful to address the issues. Third, we utilized DTI tractorgraphy to construct the WM networks. Brain networks can also be studied using structural and functional MRI data (Achard et al. 2006; He et al. 2007). The combination of these multimodal MRI techniques would yield a more comprehensive understanding of how structural disruptions in brain networks are associated with functional deficits in patients with MS. Forth, the distributions of the WM lesions were around the cerebral ventricle for all the patients, therefore we could not category the patients according to their lesion locations. Further studies would be important to explore whether and how topology alterations of WM networks are related to the spatial distribution of WM lesions in MS. Finally, it remains unclear whether the topological changes observed in RRMS can be generalized to other clinical phenotypes.

Conclusions

In the present study, we used diffusion tensor tractography and graph theoretical analyses to investigate MS-related changes in the topological efficiency in WM structural networks. We found that, compared with controls, patients with MS had a reduced network efficiency in their brain networks, with the most pronounced reduction observed in the sensorimotor, visual, default-mode, and language systems. Specifically, this reduction was correlated with the clinical characteristics of the patients. Thus, our results suggest a disrupted integrity in the large-scale brain systems in MS and provide structural insights into the MS connectome. Our data also suggest that a topology-based brain network analysis can provide potential biomarkers for disease diagnosis and the monitoring of the progression of the disease and the treatment effects for patients with MS.

Supplementary Material

Supplementary material can be found at: http://www.cercor.oxfordjournals.org/

Funding

National Science Foundation of China (Nos. 81000633, 30870667, 81030028, 30930029, and 30800267) ; the Beijing Natural Science Foundation (No. 7102090) ; the Scientific Research Foundation for the Returned Overseas Chinese Scholars (State Education Ministry, Y.H.); McDonald Fellowship from Multiple Sclerosis International Federation (MSIF, to Y.L.).

Notes

We would like to thank Chun-Yi Lo for help in the network visualization. *Conflict of Interest*: None declared.

References

Achard S, Bullmore E. 2007. Efficiency and cost of economical brain functional networks. PLoS Comput Biol. 3:e17.

Achard S, Salvador R, Whitcher B, Suckling J, Bullmore E. 2006. A resilient, low-frequency, small-world human brain functional network with highly connected association cortical hubs. J Neurosci. 26:63–72.

Au Duong MV, Audoin B, Boulanouar K, Ibarrola D, Malikova I, Confort-Gouny S, Celsis P, Pelletier J, Cozzone PJ, Ranjeva JP. 2005. Altered functional connectivity related to white matter changes inside the working memory network at the very early stage of MS. J Cereb Blood Flow Metab. 25:1245–1253.

Au Duong MV, Boulanouar K, Audoin B, Treseras S, Ibarrola D, Malikova I, Confort-Gouny S, Celsis P, Pelletier J, Cozzone PJ, et al. 2005. Modulation of effective connectivity inside the working memory network in patients at the earliest stage of multiple sclerosis. Neuroimage. 24:533–538.

Barkhof FJ, Elton M, Lindeboom J, Tas MW, Schmidt WF, Hommes OR, Polman CH, Kok A, Valk J. 1998. Functional correlates of callosal atrophy in relapsing-remitting multiple sclerosis patients. A preliminary MRI study. J Neurol. 245:153–158.

Basser PJ, Mattiello J, LeBihan D. 1994. Estimation of the effective self-diffusion tensor from the NMR spin echo. J Magn Reson. 103:247–254.

Basser PJ, Pajevic S, Pierpaoli C, Duda J, Aldroubi A. 2000. In vivo fiber tractography using DT-MRI data. Magn Reson Med. 44:625–632.

Bodini B, Khaleeli Z, Cercignani M, Miller DH, Thompson AJ, Ciccarelli O. 2009. Exploring the relationship between white matter and gray matter damage in early primary progressive multiple sclerosis: an in vivo study with TBSS and VBM. Hum Brain Mapp. 30:2852–2861.

Bullmore E, Sporns O. 2009. Complex brain networks: graph theoretical analysis of structural and functional systems. Nat Rev Neurosci. 10:186–198.

Ceccarelli A, Rocca MA, Pagani E, Colombo B, Martinelli V, Comi G, Filippi M. 2008. A voxel-based morphometry study of grey matter loss in MS patients with different clinical phenotypes. Neuroimage. 42:315–322.

Ceccarelli A, Rocca MA, Valsasina P, Rodegher M, Pagani E, Falini A, Comi G, Filippi M. 2009. A multiparametric evaluation of regional brain damage in patients with primary progressive multiple sclerosis. Hum Brain Mapp. 30:3009–3019.

Cercignani M, Inglese M, Pagani E, Comi G, Filippi M. 2001. Mean diffusivity and fractional anisotropy histograms of patients with multiple sclerosis. AJNR. 22:952–958.

Charil A, Dagher A, Lerch JP, Zijdenbos AP, Worsley KJ, Evans AC. 2007. Focal cortical atrophy in multiple sclerosis: relation to lesion load and disability. Neuroimage. 34:509–517.

Ciccarelli O, Werring DJ, Barker GJ, Griffin CM, Wheeler-Kingshott CA, Miller DH, Thompson AJ. 2003. A study of the mechanisms of normal-appearing white matter damage in multiple sclerosis using diffusion tensor imaging—evidence of Wallerian degeneration. J Neurol. 250:287–292.

Ciccarelli O, Werring DJ, Wheeler-Kingshott CA, Barker GJ, Parker GJ, Thompson AJ, Miller DH. 2001. Investigation of MS normal-appearing brain using diffusion tensor MRI with clinical correlations. Neurology. 56:926–933.

Dalton CM, Chard DT, Davies GR, Miszkiel KA, Altmann DR, Fernando K, Plant GT, Thompson AJ, Miller DH. 2004. Early development of multiple sclerosis is associated with progressive grey matter atrophy in patients presenting with clinically isolated syndromes. Brain. 127:1101–1107.

Dasenbrock HH, Smith SA, Ozturk A, Farrell SK, Calabresi PA, Reich DS. 2010. Diffusion tensor imaging of the optic tracts in multiple sclerosis: association with retinal thinning and visual disability. J Neuroimaging. doi:10.1111/j.1552-6569.2010.00468.x.

Dineen RA, Vilisaar J, Hlinka J, Bradshaw CM, Morgan PS, Constantinescu CS, Auer DP. 2009. Disconnection as a mechanism for cognitive dysfunction in multiple sclerosis. Brain. 132:239–249.

Evangelou N, Esiri MM, Smith S, Palace J, Matthews PM. 2000. Quantitative pathological evidence for axonal loss in normal appearing white matter in multiple sclerosis. Ann Neurol. 47:391–395.

Faro SH, Mohamed FB, Tracy JI, Elfont RM, Pinus AB, Lublin FD, Koenigsberg RA, Chen CY, Tsai FY. 2002. Quantitative functional MR imaging of the visual cortex at 1.5 T as a function of luminance contrast in healthy volunteers and patients with multiple sclerosis. AJNR. 23:59–65.

Filippi M, Rocca MA. 2008. Multiple sclerosis and allied white matter diseases. Neurol Sci. 3(Suppl 29):319–322.

Fink F, Klein J, Lanz M, Mitrovics T, Lentschig M, Hahn HK, Hildebrandt H. 2010. Comparison of diffusion tensor-based tractography and quantified brain atrophy for analyzing demyelination and axonal loss in MS. J Neuroimaging. 20:334–344.

Giorgio A, Palace J, Johansen-Berg H, Smith SM, Ropele S, Fuchs S, Wallner-Blazek M, Enzinger C, Fazekas F. 2010. Relationships of brain white matter microstructure with clinical and MR measures in relapsing-remitting multiple sclerosis. J Magn Reson Imaging. 31:309–316.

Gong G, He Y, Concha L, Lebel C, Gross DW, Evans AC, Beaulieu C. 2009. Mapping anatomical connectivity patterns of human cerebral cortex using in vivo diffusion tensor imaging tractography. Cereb Cortex. 19:524–536.

Gong G, Rosa-Neto P, Carbonell F, Chen ZJ, He Y, Evans AC. 2009. Age- and gender-related differences in the cortical anatomical network. J Neurosci. 29:15684–15693.

Greicius MD, Krasnow B, Reiss AL, Menon V. 2003. Functional connectivity in the resting brain: a network analysis of the default mode hypothesis. Proc Natl Acad Sci U S A. 100:253–258.

Hagmann P, Cammoun L, Gigandet X, Meuli R, Honey CJ, Wedeen VJ, Sporns O. 2008. Mapping the structural core of human cerebral cortex. PLoS Biol. 6:e159.

He Y, Chen ZJ, Evans AC. 2007. Small-world anatomical networks in the human brain revealed by cortical thickness from MRI. Cereb Cortex. 17:2407–2419.

He Y, Dagher A, Chen Z, Charil A, Zijdenbos A, Worsley K, Evans A. 2009. Impaired small-world efficiency in structural cortical networks in multiple sclerosis associated with white matter lesion load. Brain. 132:3366–3379.

He Y, Evans A. 2010. Graph theoretical modeling of brain connectivity. Curr Opin Neurol. 23:341–350.

Indefrey P, Brown CM, Hellwig F, Amunts K, Herzog H, Seitz RJ, Hagoort P. 2001. A neural correlate of syntactic encoding during speech production. Proc Natl Acad Sci U S A. 98:5933–5936.

Iturria-Medina Y, Sotero RC, Canales-Rodriguez EJ, Aleman-Gomez Y, Melie-Garcia L. 2008. Studying the human brain anatomical network via diffusion-weighted MRI and graph theory. Neuroimage. 40:1064–1076.

Kolappan M, Henderson AP, Jenkins TM, Wheeler-Kingshott CA, Plant GT, Thompson AJ, Miller DH. 2009. Assessing structure and function of the afferent visual pathway in multiple sclerosis and associated optic neuritis. J Neurol. 256:305–319.

Latora V, Marchiori M. 2001. Efficient behavior of small-world networks. Phys Rev Lett. 87:198701.

Lin F, Yu C, Jiang T, Li K, Chan P. 2007. Diffusion tensor tractography-based group mapping of the pyramidal tract in relapsing-remitting multiple sclerosis patients. AJNR. 28:278–282.

Lowe MJ, Beall EB, Sakaie KE, Koenig KA, Stone L, Marrie RA, Phillips MD. 2008. Resting state sensorimotor functional connectivity in multiple sclerosis inversely correlates with transcallosal motor pathway transverse diffusivity. Hum Brain Mapp. 29:818–827.

Lowe MJ, Phillips MD, Lurito JT, Mattson D, Dzemidzic M, Mathews VP. 2002. Multiple sclerosis: low-frequency temporal blood oxygen level-dependent fluctuations indicate reduced functional connectivity initial results. Radiology. 224:184–192.

Lublin FD, Reingold SC. 1996. Defining the clinical course of multiple sclerosis: results of an international survey. National Multiple Sclerosis Society (USA) Advisory Committee on Clinical Trials of New Agents in Multiple Sclerosis. Neurology. 46:907–911.

Lubrano V, Roux FE, Demonet JF. 2004. Writing-specific sites in frontal areas: a cortical stimulation study. J Neurosurg. 101:787–798.

Maslov S, Sneppen K. 2002. Specificity and stability in topology of protein networks. Science. 296:910–913.

Mesulam MM. 1998. From sensation to cognition. Brain. 121(Pt 6):1013–1052.

Mori S, Crain BJ, Chacko VP, van Zijl PC. 1999. Three-dimensional tracking of axonal projections in the brain by magnetic resonance imaging. Ann Neurol. 45:265–269.

Mori S, Kaufmann WE, Davatzikos C, Stieltjes B, Amodei L, Fredericksen K, Pearlson GD, Melhem ER, Solaiyappan M, Raymond GV, et al. 2002. Imaging cortical association tracts in the human brain using diffusion-tensor-based axonal tracking. Magn Reson Med. 47:215–223.

Mori S, van Zijl PC. 2002. Fiber tracking: principles and strategies—a technical review. NMR Biomed. 15:468–480.

Passamonti L, Cerasa A, Liguori M, Gioia MC, Valentino P, Nistico R, Quattrone A, Fera F. 2009. Neurobiological mechanisms underlying emotional processing in relapsing-remitting multiple sclerosis. Brain. 132:3380–3391.

Polman CH, Reingold SC, Edan G, Filippi M, Hartung HP, Kappos L, Lublin FD, Metz LM, McFarland HF, O'Connor PW, et al. 2005. Diagnostic criteria for multiple sclerosis: 2005 revisions to the "McDonald Criteria". Ann Neurol. 58:840–846.

Raichle ME, MacLeod AM, Snyder AZ, Powers WJ, Gusnard DA, Shulman GL. 2001. A default mode of brain function. Proc Natl Acad Sci U S A. 98:676–682.

Reich DS, Smith SA, Gordon-Lipkin EM, Ozturk A, Caffo BS, Balcer LJ, Calabresi PA. 2009. Damage to the optic radiation in multiple sclerosis is associated with retinal injury and visual disability. Arch Neurol. 66:998–1006.

Reich DS, Zackowski KM, Gordon-Lipkin EM, Smith SA, Chodkowski BA, Cutter GR, Calabresi PA. 2008. Corticospinal tract abnormalities are associated with weakness in multiple sclerosis. AJNR. 29:333–339.

Rocca MA, Pagani E, Absinta M, Valsasina P, Falini A, Scotti G, Comi G, Filippi M. 2007. Altered functional and structural connectivities in patients with MS: a 3-T study. Neurology. 69:2136–2145.

Rocca MA, Valsasina P, Absinta M, Riccitelli G, Rodegher ME, Misci P, Rossi P, Falini A, Comi G, Filippi M. 2010. Default-mode network dysfunction and cognitive impairment in progressive MS. Neurology. 74:1252–1259.

Roosendaal SD, Geurts JJ, Vrenken H, Hulst HE, Cover KS, Castelijns JA, Pouwels PJ, Barkhof F. 2009. Regional DTI differences in multiple sclerosis patients. Neuroimage. 44:1397–1403.

Roosendaal SD, Schoonheim MM, Hulst HE, Sanz-Arigita EJ, Smith SM, Geurts JJ, Barkhof F. 2010. Resting state networks change in clinically isolated syndrome. Brain. 133:1612–1621.
Roux FE, Dufor O, Giussani C, Wamain Y, Draper L, Longcamp M, Demonet JF. 2009. The graphemic/motor frontal area Exner's area revisited. Ann Neurol. 66:537–545.
Rovaris M, Gass A, Bammer R, Hickman SJ, Ciccarelli O, Miller DH, Filippi M. 2005. Diffusion MRI in multiple sclerosis. Neurology. 65:1526–1532.
Rovaris M, Gallo A, Valsasina P, Benedetti B, Caputo D, Ghezzi A, Montanari E, Sormani MP, Bertolotto A, Mancardi G, et al. 2005. Short-term accrual of gray matter pathology in patients with progressive multiple sclerosis: an in vivo study using diffusion tensor MRI. Neuroimage. 24:1139–1146.
Rovaris M, Judica E, Gallo A, Benedetti B, Sormani MP, Caputo D, Ghezzi A, Montanari E, Bertolotto A, Mancardi G, et al. 2006. Grey matter damage predicts the evolution of primary progressive multiple sclerosis at 5 years. Brain. 129:2628–2634.
Sailer M, Fischl B, Salat D, Tempelmann C, Schonfeld MA, Busa E, Bodammer N, Heinze HJ, Dale A. 2003. Focal thinning of the cerebral cortex in multiple sclerosis. Brain. 126:1734–1744.
Schoonheim MM, Geurts JJ, Barkhof F. 2010. The limits of functional reorganization in multiple sclerosis. Neurology. 74:1246–1247.
Sepulcre J, Goni J, Masdeu JC, Bejarano B, Velez de Mendizabal N, Toledo JB, Villoslada P. 2009. Contribution of white matter lesions to gray matter atrophy in multiple sclerosis: evidence from voxel-based analysis of T1 lesions in the visual pathway. Arch Neurol. 66:173–179.
Shu N, Liu Y, Li J, Li Y, Yu C, Jiang T. 2009. Altered anatomical network in early blindness revealed by diffusion tensor tractography. PLoS One. 4:e7228.
Sporns O, Tononi G, Kotter R. 2005. The human connectome: a structural description of the human brain. PLoS Comput Biol. 1:e42.
Tzourio-Mazoyer N, Landeau B, Papathanassiou D, Crivello F, Etard O, Delcroix N, Mazoyer B, Joliot M. 2002. Automated anatomical labeling of activations in SPM using a macroscopic anatomical parcellation of the MNI MRI single-subject brain. Neuroimage. 15:273–289.
Vishwas MS, Chitnis T, Pienaar R, Healy BC, Grant PE. 2010. Tract-based analysis of callosal, projection, and association pathways in pediatric patients with multiple sclerosis: a preliminary study. AJNR. 31:121–128.
Watts DJ, Strogatz SH. 1998. Collective dynamics of "small-world" networks. Nature. 393:440–442.
Westin CF, Maier SE, Mamata H, Nabavi A, Jolesz FA, Kikinis R. 2002. Processing and visualization for diffusion tensor MRI. Med Image Anal. 6:93–108.
Yu CS, Lin FC, Liu Y, Duan Y, Lei H, Li KC. 2008. Histogram analysis of diffusion measures in clinically isolated syndromes and relapsing-remitting multiple sclerosis. Eur J Radiol. 68:328–334.
Zalesky A, Fornito A. 2009. A DTI-derived measure of cortico-cortical connectivity. IEEE Trans Med Imaging. 28:1023–1036.